

An Automatic Media-Adventitia Border Segmentation Approach for IVUS Images

Matheus Cardoso Moraes¹, Sergio Shiguemi Furuie¹

¹ School of Engineering, University of São Paulo, Brazil

Abstract

In image processing, segmentation is considered one of the most important and hardest operations. The media-adventitia segmentation, in Intravascular Ultrasound (IVUS) images, is one of the first steps for a vase 3D reconstruction, and it is an important operation for many applications: measurements of its border circumference, area and radius; for studies about the mechanical properties and anatomical structures of vessels; which consequently will infer about therapy plans and evaluations; localization of pathologies. The purpose here is to segment the media-adventitia in IVUS images with high accuracy by combining a set of imaging-processing techniques: Speckle Reducing Anisotropic Diffusion (SRAD), Wavelet, Otsu and Mathematical Morphology. Firstly, SRAD is applied to attenuate the speckle noises. Next, the vessel and plaque features are extracted by performing Wavelet Transform. Optimal thresholding is carried out by Otsu to create a binarized version of these features. Then, Mathematical Morphology is used to obtain an adventitia shape. Finally, this approach is evaluated by segmenting 100 challenging images, obtaining an average of True Positive (TP(%)) = 92.83 ± 4.91 , False Positive (FP(%)) = 3.43 ± 3.47 , False Negative (FN(%)) = 7.17 ± 4.91 , Max False Positive (Max_{FP}(mm)) = 0.27 ± 0.22 , Max False Negative (Max_{FN}(mm)) = 0.31 ± 0.2 . Futhermore, its effectiveness is demonstrated by comparing this result with a recent one in the literature.

1. Introduction

Yearly, over 250,000 lives are lost in USA by atherosclerosis [4]. Intravascular ultrasound (IVUS) is a medical imaging modality, which provides anatomical, morphological, and some pathological information of coronary arteries and plaques. Thus, it is employed in most cardiac procedures [5,7]. Likewise, its image segmentation is not only known to be one of the steps for a vase 3D reconstruction, yet it can also help health professionals to study vessel and plaques characteristics, mechanical properties, anatomical structures, tissue qualification and volume quantification,

internal and external wall perimeter and radius, and location of pathologies. Accordingly, it results in more precise diagnostic, therapy plans and evaluations [2, 9, 12]. Two different IVUS-image segmentation methods are described in [5, 12]; the former is based on Discrete Wavelet Packet Frame (DWPF) [1], k-means and the spline interpolation, while the latter relies on Principal Components Analysis (PCA), and an energy minimization process. Again, a simple, reliable and automatic method to segment the m-a border in IVUS images is proposed herein.

2. Methods

The Material is from the Heart Institute of São Paulo Brazil (InCor), and consists of 100 challenging IVUS images from 24 patients - with different vessel and plaques features.

The Method consists in segmenting the media-adventitia borders by accomplishing the following stages: pre-processing, processing, and post-processing, as summarized below:

1. Pre-processing:
 - (a) Image size and resolution normalization;
 - (b) Transducer reflection attenuation;
 - (c) Speckle Filtering;
 - (d) Conversion to the polar domain.
2. Processing:
 - (a) Feature extraction using DWPF;
 - (b) Binarization using Otsu;
 - (c) Morphological Combination.
3. Post-processing:
 - (a) Branch-opening test and correction;
 - (b) Return to the Cartesian domain;
 - (c) Adventitia-Contour extraction (Segmentation Concluded).

2.1. Pre-processing

The **pre-processing stage** is shown to make the image ready for being processed, by respectively minimizing and maximizing the undesirable and desirable image features. It begins with a 400×400 **Image size and resolution nor-**

malization followed by a **Transducer reflection attenuation**:

$$I_{NR} = \begin{cases} \frac{I_O}{10}, & \text{if } rad < 41 \text{ pix} \\ \left(\frac{I_O}{10}\right) (rad - 40), & \text{if } (41 \leq rad < 51) \text{ pix} \\ I_O, & \text{otherwise} \end{cases}, \quad (1)$$

where I_O and I_{NR} are respectively the pixels' intensities of the original and no reflection image, rad is the radius to current processed pixel. This procedure does not create new borders. Next, **Speckle filtering**, "Speckle Reducing Anisotropic Diffusion" (SRAD) [13] takes place to attenuate the Speckle noise, using: Windows size in an homogeneous region (40×40), Number of interactions $n = 100$, $\Delta t = 0.5s$. A **Conversion to the polar domain**, ($I_{Polar}(r, \theta)$) helps the computational process [12], and concludes this section (Figure 1(a)).

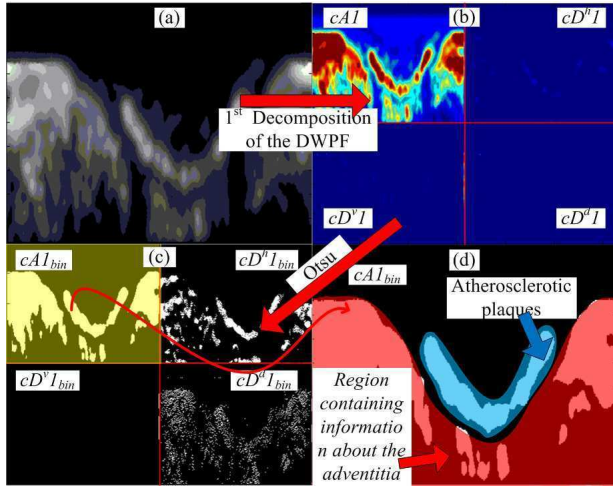


Figure 1. (a) Illustration of an Image in the Polar Domain (r, θ), after going through the Pre-Processing stage. (b) 1st decomposition. coefficients of the DWPF. (c) Wavelets' coefficients binarized using Otsu. (d) Zoom at the $cA1_{bin}$ coefficient, which contains the most relevant information regarding plaques and adventitia.

2.2. Processing

In order to obtain an adventitia shape APO_{bin} (Figure 2(i)); firstly, the plaque and vessel features must be extracted from the pre-processed image; secondly, a binarized version of this features will have to be created, thus it could be finally worked to be improved.

Feature extraction using DWPF - The vessel and plaque information are extracted using Discrete Wavelet Packet Frame (DWPF) [1, 4, 5], Daubechie 1 (dB1) and 1 decomposition level of binary tree structure [6, 8], (Figure 1(b)) were used.

Binarization using Otsu - A binarized version of the resultant wavelets' coefficients were created, $cA1_{bin}$, cD_{bin}^h , cD_{bin}^v , and cD_{bin}^d (Figure 1(c)), aiming to improve the known information and estimating the missing ones. Otsu's [10] was used for optimum thresholding, seeing that the coefficient histograms are quite bi-modal.

Morphological Combination - The $cA1_{bin}$ is shown to be the binary image that has the most complete plaque and adventitia information (Figure 1(d) in blue and red). Therefore, it will be used to generate the APO_{bin} (Figure 2(i)), using Mathematic Morphology [3]. This procedure consists in creating and combining three complementary images: Tissue Information (T_{inf}) (Figure 2(b)), Adventitia Missing Region Information (A_{mis}) (Figure 2(c)) and Skeleton (Skt) (Figure 2(d)). The **Complementary Images 1** or T_{inf} (Figure 2(b)) is obtained by an opening operation between the $cA1_{bin}$ and a structuring element ($S_{2 \times 50}$) with 2 lines and 50 columns filled by ones.

$$T_{inf} = cA1_{bin} \circ S_{2 \times 50}. \quad (2)$$

The reason of this operation, and this structuring element dimension, is to separate the plaques from the adventitia, so that the first could be removed by area selection in later operations. **Complementary Image 2** or A_{mis} (Figure 2(c) shows the $cA1_{bin}$ -adventitia missing information (Figure 2(a) highlighted in yellow). This estimation is obtained by; firstly, applying 10 times a thickening procedure (ϕ) of 1 pixel (S_1) over $cA1_{bin}$

$$cA1_{binThick} = ((\dots ((cA1_{bin} \phi S_1^1) \phi S_1^2) \dots) \phi S_1^{10}); \quad (3)$$

next, performing an upward filling procedure at $cA1_{binThick}$, where its columns are filled with ones upwardly until the first white pixel.

$$A_{mis} = Fill_{upward}(cA1_{binThick}). \quad (4)$$

Complementary Image 3 or Skt (Figure 2(d)) is known to be the structure, which connects only the adventitia objects, for the latter binary selection. This skeleton is created by

$$Skt = \bigcup_{k=0}^K S_k(CF_{down}), \quad (5)$$

where S_k is a skeleton procedure, and CF_{down} is given by:

$$CF_{down} = Fill_{down}(cA1_{bin} \bullet S_{10 \times 100}), \quad (6)$$

where $Fill_{down}$ is a downwards filling procedure and \bullet is a closing operation between $cA1_{bin}$ and $S_{10 \times 100}$.

Final Polar Domain Image - The complete adventitia shape in the polar domain APO_{bin} (Figure 2(g)), is obtained by; firstly, unifying the mentioned three complementary images (Figure 2(e))

$$U = T_{inf} \cup A_{mis} \cup Skt; \quad (7)$$

secondly, removing the plaques from the image by using binary area selection, $B_{selected}$ (Figure 2(f)), and; finally, the Adventitia Polar Object (APO_{bin}) (Figure 2(g)) is obtained using:

$$APO_{bin} = (B_{selected} \bullet S_{circular(50)}), \quad (8)$$

where the structuring element $S_{circular(50)}$ is a special matrix that disposes the ones in a circular way with 50 pixel diameter.

2.3. Post-processing

Test and correction of Side Branches - For a signal $h(\theta_i)$ representing the column height of the APO_{bin} ,

$$h(\theta_i) = \sum_j APO_{bin}(r_j, \theta_i), \quad (9)$$

and given two derivatives of this signal, higher than a certain threshold. The branch correction is performed by computing an interpolation between these two derivatives; afterwards, this signal goes back to the binary image domain.

Returning to the Cartesian Domain - A Cartesian domain image is generated $I_{Cartesian}$ (Figure 2(h)) from the APO_{bin} .

Adventitia Contour Extraction - The segmentation is concluded by extract the $I_{Cartesian}$ contour, using:

$$\beta(I_{Cartesian}) = I_{Cartesian} - (I_{Cartesian} \varepsilon S_{3 \times 3}), \quad (10)$$

where ε represents an erosion procedure, and placing it at the $I_{Original}$, generating I_{Final} (Figure 2(i)):

$$I_{Final} = \beta(I_{Cartesian}) \cup I_{Original}. \quad (11)$$

3. Results

Some visual result from the dataset mentioned in the methodology can be seen in Figure 3 (a), (b) and (c), and its manual segmentation respectively in Figure 3 (d),(e) and (f), made by an expert (Gold Standard). According to [11], we compute the rate of True Positive (TP), False Positive (FP), False Negative (FN), Maximum Positive Deviation (Max_{FP}) and Maximum Negative Deviation (Max_{FN}) (Table 1). Nonetheless, in order to compare this result with the one obtained by [12], our index were taken to theirs: Overlap Ratio (OR) [$OR=TP/(TP+FN+FP)$]; False Positive Rate (FPR) [$FPR=FP/(FP+TN)$]; False Negative Rate (FNR) [$FNR=FN/(FN+TP)$], and Maximum Distance

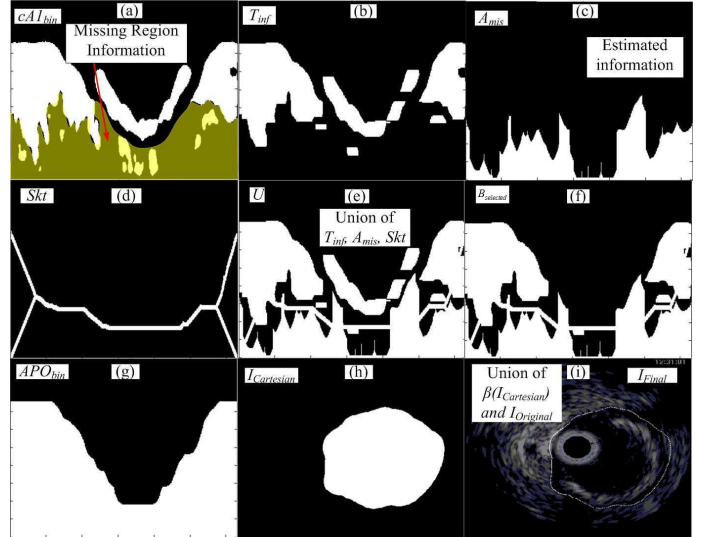


Figure 2. (a) $cA1_{bin}$ with the missing adventitia information highlighted. (b) Complementary image 1, T_{inf} , shows the obtained information about the the plaques and adventitia, including the separation between them. (c) Complementary image 2, A_{mis} , shows a estimation of the adventitia missing information. (d) Complementary image 3, Skt , shows a structure that can only connect the information related to the adventitia. (e) Union of the three complementary images. (f) The remained adventitia information, after a binary selection, using region growing. (g) Adventitia polar image, APO_{bin} , shows the adventitia object in the polar domain, obtained after a closing procedure in (f). (h) Adventitia Cartesian image, $I_{Cartesian}$, shows the logic negation of the adventitia shape in the Cartesian domain. (i) Final image, I_{Final} , shows the final result of the adventitia segmentation, after extracting the contour from (h), $\beta(I_{Cartesian})$, and place it in the original Image, $I_{Original}$.

($Max_{Distance}$) [$Max_{Distance}=\max(Max_{FP}, Max_{FN})$] (Table 2).

4. Discussion and conclusions

As can be seen, Table 2 (Unal Method 1) provides the best result, as it used a set of images with minor calcification and branch opening, images assumed to be easily segmented. Conversely, in Table 2 (Unal Method 2), the result suffered a degradation, because it used not only the previous dataset, but also some challenging images, with large calcification and branch opening, which represents 34% of the total set. In our dataset, there are images with and without branches, different vessel sizes; moreover, 88% of the images have calcified, fibrotic and lipidic plaques. Therefore, our resulting Table 2 (Proposed Approach), could be fairly compared to the (Unal Method 2), which gives an

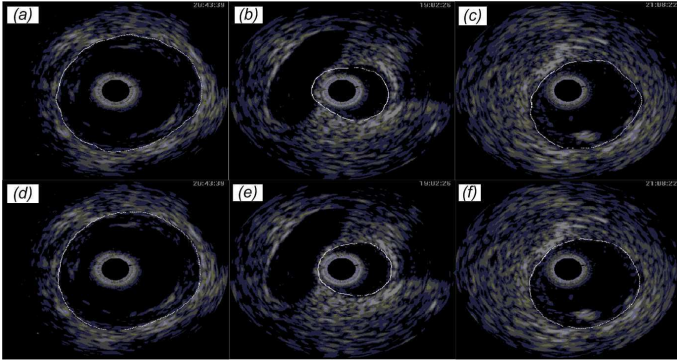


Figure 3. (a), (b) and (c) are some of IVUS-image segmentation examples made by this automated method. Respectively (d), (e) and (f) are their correspondent images segmented by an expert used as Gold Standards.

Table 1. Assessment of the proposed approach for 100 images using the index suggested by Udupaet al.

Index Used by Udupa	Parameters				
	TP (%)	FP (%)	FN (%)	Max _{FP} (mm)	Max _{FN} (mm)
Proposed	92.83	3.43	7.17	0.27	0.31
Approach	±4.91	±3.47	±4.91	±0.22	±0.2

advantage to them, respectively, less than 1% and 2% at the OR(%) and FNR(%), yet the proposed approach provides smaller standard deviation and Max_{Distance} (Table 2). In general, one can say that both methods have similar results. Nonetheless, ours is simpler computationally, since it does not have to compute large covariance and estimation of PDFs.

This paper presented a new segmentation method, the result of which justifies its use, our contribution were: a) Catheter reflection attenuation; b) A combination of techniques (SRAD, DWPF, Otsu) and the optimum parameters, which led to tissue and plaques feature extracted; c) Morphological operations to create a adventitia shape; d) segmentation results of challenging images. For future work, the association of other parameters to segment the Lumen will be investigated.

Acknowledgments

CNPq (National Council of Scientific and Technological Development - Brazil), **InCor** (Heart Institute of São Paulo - Brazil), **LEB-USP** (Biomedical Engineering Laboratory of the State University of São Paulo - Brazil).

References

[1] Ronald R. C, Mladen V. W. Entropy-based algorithms for best basis selection. IEEE Transaction on Information Theory 1992;38:713–8.

Table 2. Result comparison among the methods and parameters of three different datasets using the index suggested by Unal et al.

Index Used by Unal	Parameters		
	OR (%)	FNR (%)	Max _{Distance} (mm)
Unal	92.23	5.35	0.84
Method 1	±6.27	±7.86	±1.74
Unal	90.57	5.55	0.98
Method 2	±10.66	±9.20	±1.78
Proposed	89.79	7.17	0.31
Approach	±4.51	±4.91	±0.2

[2] Milan S, J. Michael F. Handbook of Medical Imaging: Medical Image Processing and Analysis. Bellingham, WA: SPIE Press, 2000;2: Chap. 2-3, Image Segmentation - Image Segmentation Using Deformable Models.

[3] Rafael C. G, Richard E. W. Digital Image Processing. 3rd ed, New Jersey, Pearson Prentice Hall, 2008: Chap. 9 - Morphological Image Processing.

[4] Amin K, Babak B, Elisa E. K, Andrew F. L. Texture-driven coronary artery plaque characterization using wavelet packet signatures. In: IEEE International Symposium on Biomedical Imaging: From Nano to Macro, 2008;5:197–00

[5] Amin K, Babak B, Elisa E. K, Andrew F. L. Automatic detection of blood versus non-blood regions on intravascular ultrasound (IVUS) images using wavelet packet signatures. In: Medical Imaging 2008: Ultrasonic Imaging and Signal Processing, 2008, San Diego, CA, USA.

[6] Stéphane M. A Wavelet Tour of Signal Processing: The Sparse Way. 3rd.ed. New York: Academic Press, 2009: Chap. 8 - Wavelet Packet and Local Cosine Bases.

[7] Roch L. M, Jacques O, Gérard F, Guy C. Adapting the Lagrangian speckle model estimator for endovascular elastography: Theory and validation with simulated radio-frequency data. Journal of Acoustic Society of America, 2004;116:1276–86

[8] Michel M, Yves M, Georges O, Jean-Michel P. Wavelet Toolbox User's Guide Version 2. The Math Work Inc., 2000: Chap. 1 - Wavelets: A New Tool for Signal Analysis.

[9] László G. N, Alexandre X. F, Jayaram K. U. Fuzzy-connected 3D image segmentation at interactive speeds. Elsevier on Graphical Models, 2003;64:259–81.

[10] Nobuyuki O. Threshold selection Method from Gray-Level Histograms. IEEE Transactions on Systems Man and Cybernetics, 1979;9:62–66.

[11] Jayaram K. U, Vicki R. L, Hilary S, Celina I, Punam K. S, George J. G, Ying Z, Pat M, Yinpeng J, Leanne M. C. A Methodology for Evaluating Image Segmentation Algorithms. In: SPIE Medical Imaging, 2002. San Diego, CA, USA.

[12] Gozde U, Susann B, Stephane C, Greg S, Tong F, Kaoru T. Shape-Driven Segmentation of the Arterial Wall in Intravascular Ultrasound Images. IEEE Transactions on Information Technology in Biomedicine, 2008;12:335–47.

[13] Yongjian Y. Scott T. A. Speckle Reducing Anisotropic Diffusion. IEEE Transactions on Image Processing 2002;11:1260–70.

Address for correspondence:

Names:Matheus Cardoso Moraes

Postal address: Laboratório de Engenharia Biomédica - Departamento de Telecomunicações e Controle - Escola Politécnica da USP - Av. Prof. Luciano Gualberto, Travessa 3, 158 - sala D2-06 CEP 05508-970 São Paulo - SP - Brazil

E-mail address: matheuscardsomg@hotmail.com